Development and Validation of Cr Diffusion Model for Coated Zircaloy Accident Tolerant Fuel Cladding

Dongju Kim, Youho Lee *
Seoul National University, 1 Gwanak-ro, Gwanak-gu, Seoul 08826, Korea
**Corresponding author: leeyouho@snu.ac.kr*

1. Introduction

Zirconium alloy (Zr alloy) has been long used in pressurized-light water reactors (PWRs) as a cladding material because of its suitable mechanical property and low neutron absorption. However, it reacts rapidly with high-temperature steam under accident conditions such as loss-of-coolant accident (LOCA). Hence, after the Fukushima accident, it has drawn a strong need for developing accident-tolerant fuels (ATFs), which can significantly decrease steam oxidation rate and hydrogen generation during the accidents. The most promising concept among the probable ATFs is Cr-coated Zr alloy, in which a thin chromium layer is coated to the outer surface of nuclear fuel cladding. The application of Cr-coating can effectively reduce the high-temperature steam oxidation without significantly degrading the mechanical property of cladding or neutron economy of a reactor core [1-3].

On the other hand, high-temperature tests of Cr-coated cladding reveal the diffusion behavior of chromium [4, 5], which poses a potential degradation of cladding. For the binary Zr-Cr system, 1332 ℃ is identified as eutectic temperature. Hence, Cr-coated cladding would melt under significantly lower temperature than the melting point of uncoated Zr alloy cladding (1850 ℃ for Zircaloy-4) [6]. In addition, diffusion of chromium formed a Cr-Zr interlayer ($ZrCr_2$) between Cr-coating/Zr matrix and $ZrCr_2$ precipitation in Zr matrix after quenching [4]. $ZrCr_2$ layer and precipitation are intrinsically brittle phases, so they can act as crack propagation paths and degrade the mechanical property of cladding. Therefore, to quantitatively evaluate the increased safety margin during design-basis accidents (DBAs) or beyond-DBA by an application of Cr-coating, the degree of chromium diffusion and its impact on cladding ductility should be accounted for.

In such a context, this study aims at developing and validating a mechanistic Zr-Cr binary diffusion model for Cr-coated Zr-Nb alloy cladding. The model solves the radial diffusion equation with the Finite Difference Method (FDM) with phase changes according to the Zr-Cr phase diagram. The chromium diffusion coefficients of each phase (Zr, $ZrCr_2$) were obtained from isothermal (1000-1300 ℃) diffusion kinetics. The model has been validated with experimental results in terms of phase thicknesses and chromium concentration profile.

2. Development of Model

2.1 Governing Equation and Boundary Conditions

The radial diffusion equation ($\frac{\partial C}{\partial t} = \frac{\partial}{r\,\partial r}(Dr\frac{\partial C}{\partial r})$) was implemented as discretized form (**Eq. (1)**) with time interval dt and position interval h to calculate the chromium diffusion profile. D_i and C_i denote the diffusion coefficient and chromium concentration of i^{th} node, respectively.

$$\frac{C_i^n - C_i^{n-1}}{dt} = \frac{D_{i+1}C_{i+1}^n - (2*D_i)C_i^n + D_{i-1}C_{i-1}^n}{h^2} + D_i\frac{C_{i+1}^n - C_{i-1}^n}{2*r(i)*h} \quad (1)$$

Cladding is divided into 10000 radial meshes, and each mesh is classified as one of Cr, $ZrCr_2$, and Zr (**Fig. 1**). The chromium concentration boundary conditions (**Eq. (2)-(6)**) were applied based on the Zr-Cr phase diagram [6]. The chromium concentration of the Cr-coating layer and both boundaries of $ZrCr_2$ layer were set to a constant value (**Eq. (2)-(4)**). The chromium concentration of Zr matrix contacts with the $ZrCr_2$ layer was set to a function of temperature (**Eq. (5)**). The initial chromium concentration was set to 100 at% for the Cr-coating layer ($r < \delta_{Cr-coating}$) and 0 at% for the Zr alloy ($r < \delta_{Cr-coating}$), accords to the composition of Zr-Nb alloy (**Eq. (6)**) [7]. The movement of layer boundaries (ε_i) was modeled by the mass balance of chromium at the interface (**Eq. (7)**).

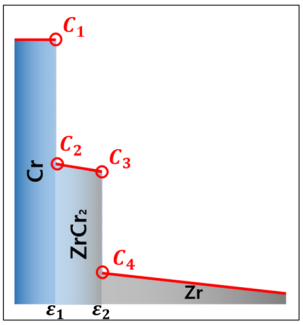

Fig. 1. Schematic boundary conditions of the model.

$$C_1(\varepsilon_1, t) = 100\ [at\%] \quad (2)$$

$$C_2(\varepsilon_1, t) = 68.7\ [at\%] \quad (3)$$

$$C_3(\varepsilon_2, t) = 63.7\ [at\%] \quad (4)$$

$$C_4(\varepsilon_2, t) = \begin{cases} 7E-6T^2-0.003T-0.7133\ [at\%] & (T > 836\ ℃) \\ 0.49\ [at\%] & (T \le 836\ ℃) \end{cases} \quad (5)$$

$$C(r,0) = \begin{cases} 100\ [at\%] & (r < \delta_{Cr-coating}) \\ 0\ [at\%] & (r > \delta_{Cr-coating}) \end{cases} \quad (6)$$

$$\frac{d\varepsilon_i}{dt} = \frac{J_i^+ - J_i^-}{C_i - C_{i+1}} \quad (7)$$

2.2 Model Numerical Scheme

The numerical scheme of our chromium diffusion model is illustrated in **Fig. 2**. For the given temperature profile, initial chromium content, and Cr-coating thickness, the model first calculates the thickness of each layer using **Eq. (7)**. Then, the code determines the phase and the diffusion coefficient of each mesh. By generating and solving the tridiagonal matrix of discretized diffusion equation (**Eq. (1)**), the model calculates the chromium distribution for the next timestep. The size of timestep is controlled to ensure the convergence of the calculated result.

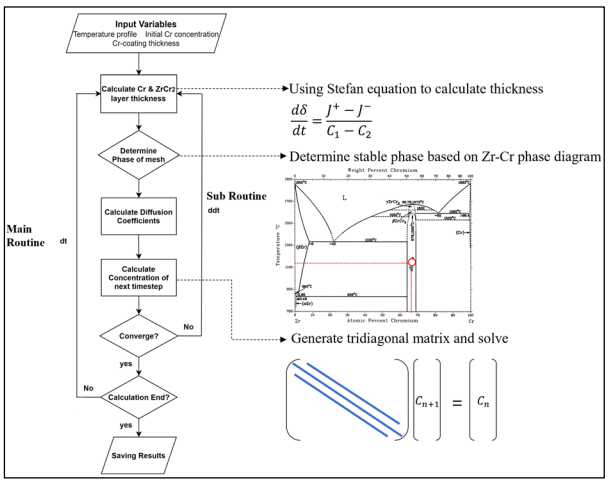

Fig. 2. Flow chart of the numerical scheme of the chromium diffusion model.

2.3 Determination of Diffusion Coefficients

The chromium diffusion coefficients of Zr and $ZrCr_2$ layers were determined to give the best agreement with isothermal (1000-1300 °C) diffusion kinetic data (layer thicknesses, chromium concentration distribution) obtained from this study. The obtained chromium diffusion coefficients were fitted in Arrhenius form, as shown in **Fig. 3**.

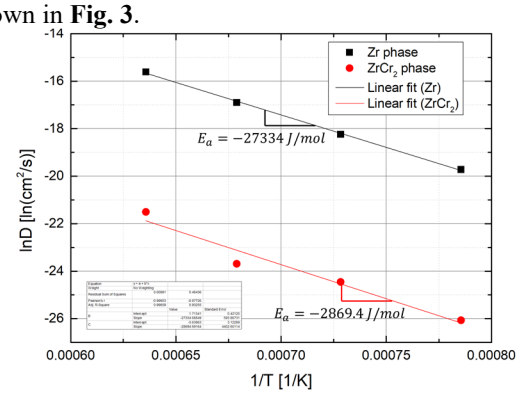

Fig. 3. Arrhenius fitting of chromium diffusion coefficients of Zr and $ZrCr_2$ phase.

3. Validation of Model

3.1 Experimental Conditions

A Cr-Zr binary diffusion experiment was conducted by exposure of Cr coated cladding to high-temperature under an inert (Ar) gas environment using a Differential Scanning Calorimeter (DSC). The Cr-coating thickness of the cladding specimen was measured to 19.5 ±0.19 μm. The cladding tube was cut into 4*4 mm size, and the weight of each specimen was 37±0.7 mg. Each specimen was heated up to the target temperature (1000-1300 °C) under the heating rate of 50 °C/min, and it was exposed isothermally for 0.25-24 h, dependent on temperature. After exposure to high temperature, each specimen was analyzed using Scanning Electron Microscope (SEM) and Electron Probe MicroAnalysis (EPMA).

3.2 Cr Concentration Distribution

The chromium concentration distribution of each specimen was measured by EPMA (JXA-8530F) after mechanical polishing. **Fig. 4 (a)** and **(b)** compare the measured EPMA chromium profile and calculated profile by model. Since there was no available data about precipitation kinetics of $ZrCr_2$, the current version of the model can choose the calculation option for precipitation. The non-equilibrium calculation assumes no $ZrCr_2$ precipitation occurs for the chromium content exceeds the solubility limit, while the equilibrium calculation assumes immediate precipitation for excessive chromium content. The final version of the model would apply the precipitation kinetics of the $ZrCr_2$ phase, and its result will be a value between these two results. Nevertheless, the current model showed remarkable agreement with experiments.

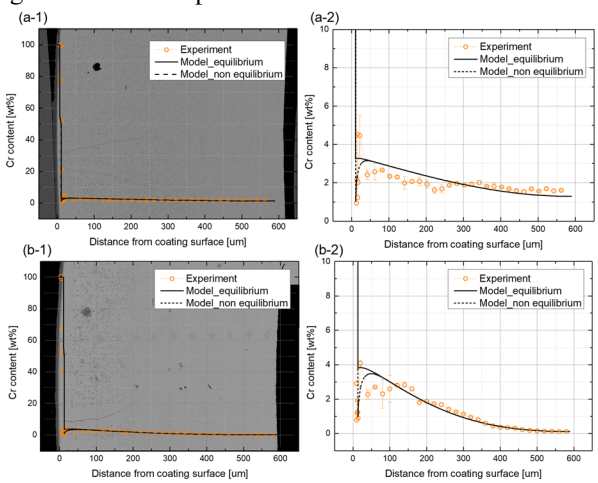

Fig. 4. Comparison of calculated chromium distribution and experimental result: (a-1), (a-2) Exposed to 1200 °C for 6h; (b-1), (b-2) Exposed to 1300 °C for 0.5h. (a-2) and (b-2) represents magnified for Zr matrix of (a-1) and (b-1).

3.3 Phase Thicknesses

Fig. 5 (a) and **(b)** are the comparison of measured thicknesses and calculated thicknesses of each phase (Zr and $ZrCr_2$) after high-temperature exposure. As shown in **Fig. 5 (a)**, the model gives good predictions for

chromium coating thickness under various temperatures (1000-1300 ℃). **Fig. 5 (b)** is the comparison result for the $ZrCr_2$ intermetallic layer thickness, and it shows that most calculated results were consistent with experiments within an error of 1 μm. Considering that the thickness of the $ZrCr_2$ layer is very thin compared to the initial Cr-coating (19.5 μm), and it was formed as an irregular shape rather than a uniform layer, the model's predictions are quite accurate.

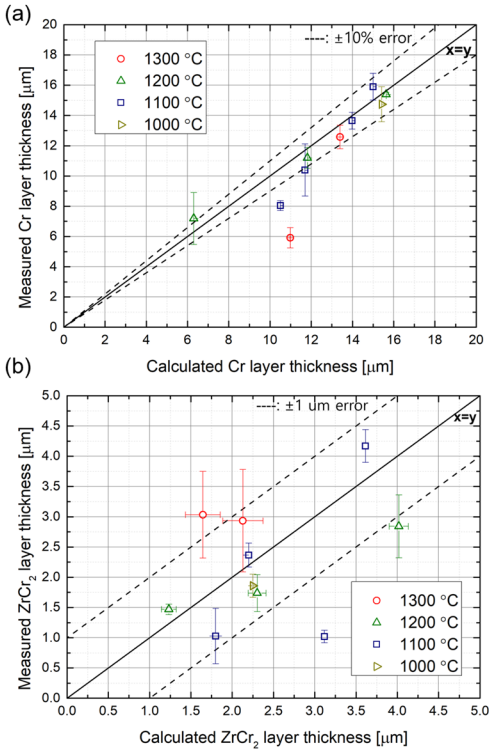

Fig. 5. Comparison of calculated phase thickness and experimental result: (a) Chromium coating layer; (b) $ZrCr_2$ intermetallic layer.

4. Implication of Cladding Integrity

4.1 Eutectic Melting

The potential Zr-Cr eutectic reaction followed by chromium diffusion, which may occur at high temperatures (>1300 ℃), is an important safety issue for Cr-coated cladding. In this study, calorimetric measurement under an inert (Ar) gas environment using DSC was conducted to ascertain the occurrence and microstructural effect of eutectic reaction. The specimen was exposed from 20 to 1400 ℃ under the heating rate of 5 K/min. After the high-temperature exposure, SEM and EDS analyses were conducted to observe its microstructure and compositional distribution.

Fig. 6 (a) shows a part of the thermogram obtained of Cr-coated cladding. The eutectic reaction is clearly shown in the endothermic peak with an onset temperature of ~1312.4 ℃. **Fig. 6 (b)** and **(c)** are the SEM images with the EDS mapping and line scan results, respectively. They clearly show the effect of eutectic melting on the microstructure of the cladding. The chromium was diffused to the center of the cladding, and numerous cavities were formed near the Cr-coating, which can stimulate the crack propagation of cladding. Furthermore, cladding thickness was increased from ~600 μm to 720 μm. The expansion of cladding could block the coolant path and impede the long-term cooling of the reactor core after accidents.

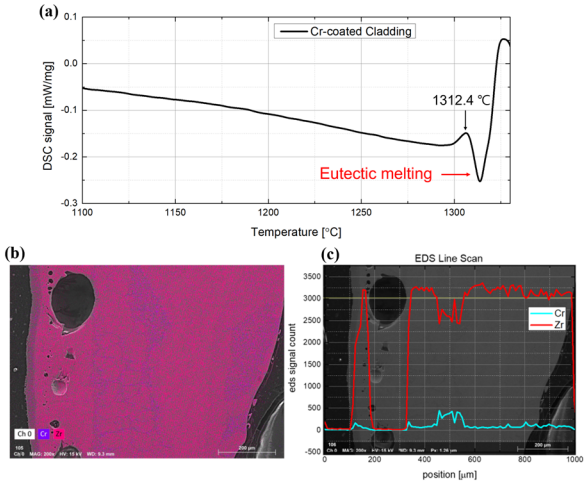

Fig. 6. Results of eutectic melting: (a) DSC signal; (b) EDS mapping results for zirconium and chromium; (c) EDS line scan results for zirconium and chromium.

4.2 Precipitation Hardening

The chromium diffused into the Zr matrix at high temperature was precipitated as $ZrCr_2$ after cooling to room temperature, as shown in **Fig. 7**. Since the $ZrCr_2$ intermetallic phase has higher hardness and is intrinsically brittle, precipitation could embrittle the Zr matrix.

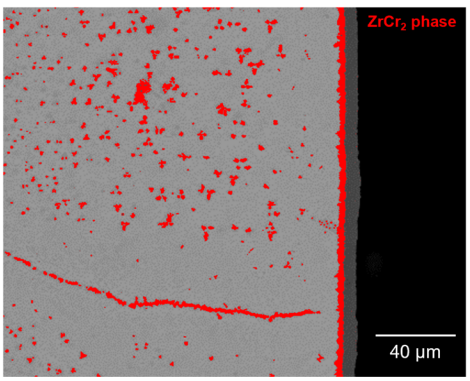

Fig. 7. SEM backscattered cross-sectional image of Cr-coated cladding after high-temperature exposure (ZrCr2 phase was marked in red by ImageJ software).

The Vickers microhardness measurement (HM-210) was conducted to correlate the microhardness and amount of $ZrCr_2$ precipitation, which is proportional to chromium concentration. As can be seen in **Fig. 8**, the hardness of the Zr matrix tends to increase with Cr content. **Eq. (8)** is a linear fitting of the correlation between chromium concentration and hardness.

$$Hardness \quad [Hv] = 11.535 * [Cr][wt\%] + 204.27 \qquad (8)$$

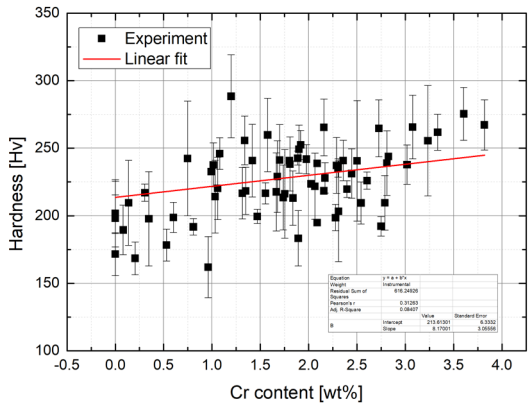

Fig. 8. Correlation between measured chromium concentration and microhardness.

5. Conclusions

In this study, a mechanistic model for chromium distribution in Cr-coated Zr-Nb alloy cladding under Zr-Cr binary system was developed and validated. The model solves the radial diffusion equation with FDM with phase changes according to the Zr-Cr phase diagram. The chromium diffusion coefficients of each phase (Zr, $ZrCr_2$) were obtained from isothermal (1000-1300 ℃) diffusion kinetics. The model has been validated in terms of phase thicknesses and chromium concentration profile of high-temperature exposed Cr-coated cladding.

Furthermore, this study finds two potential degrading mechanisms of Cr-coated cladding: eutectic melting and precipitation hardening. Throughout the DSC measurements, this study confirms the eutectic melting of Cr-coated cladding at 1312 ℃. SEM and EDS analyses of Cr-coated cladding after eutectic melting shows the numerous vacancies and relocation of cladding, which can significantly affect the safety of reactor core after accidents. The microhardness analyses of Cr-coated cladding show $ZrCr_2$ precipitation, proportional to chromium concentration, limitedly embrittle the Zr matrix.

Acknowledgments

This work was supported by the Nuclear Safety Research Program through the Korea Foundation Of Nuclear Safety(KoFONS) using the financial resource granted by the Nuclear Safety and Security Commission(NSSC) of the Republic of Korea. (No.2101051). The Cr-coated Zr-Nb alloy Cladding was provided by KEPCO Nuclear Fuel.

REFERENCES

[1] H. Yook, K. Shirvan, B. Phillips, Y. Lee, Post-LOCA ductility of Cr-coated cladding and its embrittlement limit, Journal of Nuclear Materials 558 (2022) 153354.

[2] J.C. Brachet, M. Le Saux, J. Bischoff, H. Palancher, R. Chosson, E. Pouillier, T. Guilbert, S. Urvoy, G. Nony, T. Vandenberghe, A. Lequien, C. Miton, P. Bossis, Evaluation of Equivalent Cladding Reacted parameters of Cr-coated claddings oxidized in steam at 1200 °C in relation with oxygen diffusion/partitioning and post-quench ductility, Journal of Nuclear Materials 533 (2020) 152106.

[3] J.C. Brachet, S. Urvoy, E. Rouesne, G. Nony, M. Dumerval, M.L. Saux, F. Ott, A. Michau, F. Schuster, F. Maury, DLI-MOCVD CrxCy coating to prevent Zr-based cladding from inner oxidation and secondary hydriding upon LOCA conditions, Journal of Nuclear Materials 550 (2021) 152953.

[4] J. Yang, M. Steinbrück, C. Tang, M. Große, J. Liu, J. Zhang, D. Yun, S. Wang, Review on chromium coated zirconium alloy accident tolerant fuel cladding, Journal of Alloys and Compounds 895 (2022) 162450.

[5] H.-B. Ma, J. Yan, Y.-H. Zhao, T. Liu, Q.-S. Ren, Y.-H. Liao, J.-D. Zuo, G. Liu, M.-Y. Yao, Oxidation behavior of Cr-coated zirconium alloy cladding in high-temperature steam above 1200 °C, npj Materials Degradation 5(1) (2021) 7.

[6] K.P. Gupta, The Cr-Ni-Zr (Chromium-Nickel-Zirconium) System, Journal of Phase Equilibria and Diffusion 31(2) (2010) 191-193.

[7] H.-G. Kim, J.-Y. Park, Y.-I. Jung, D.J. Park, Y.-H. Koo, Irradiation test results of HANA cladding in HALDEN test reactor after 67 GWD/MTU, 2012.